J. Fluid Mech. (1985), *vol.* 161, *pp.* 239–248
Printed in Great Britain

Three-dimensional vortex patterns in a starting flow

By P. FREYMUTH, F. FINAISH AND W. BANK
Department of Aerospace Engineering Sciences, University of Colorado, Boulder, Colorado 80309

(Received 17 January 1985 and in revised form 14 June 1985)

Vortical-pattern visualization for the starting flow behind airfoils is extended from a chordwise or two-dimensional mode to a spanwise or three-dimensional mode. We demonstrate the capabilities and limits of the extended method by means of selected photographic frames and sequences.

1. Introduction

Chordwise vortical-pattern visualizations in a starting flow of constant acceleration around an airfoil by Freymuth, Bank & Palmer (1983*a*, 1984, 1985) yielded detailed resolution of vortical shapes in two dimensions. No visualization in the third spanwise dimension is needed as long as the flow remains two-dimensional. Some time after flow start-up, however, chordwise vortical patterns become blurred, indicating the onset of turbulence. To look into the two-dimensionality of the initial vortical developments and to resolve three-dimensional effects during the transition to turbulence, we extended our flow visualization from a chordwise cross-section to the spanwise dimension. A display of three-dimensional vortical patterns is given to demonstrate our current abilities. No previous information on three-dimensional effects in a starting flow is available: therefore, the literature on related phenomena in better-known flow configurations must serve as a reference of comparison.

2. Visualization method

Our visualization of vortical structures in a chordwise cross-section and applied to starting flows has been described in detail by Freymuth, Bank & Palmer (1983*b*). Visualization of spanwise vortical structure is achieved by a rather elementary modification of the method. The spanwise axis of the NACA 0015 airfoil is remounted from a horizontal position, as shown in figure 1 (*a*), to a vertical position as shown in figure 1 (*b*). The airfoil tips fitted nearly flush with the top and bottom walls of the tunnel, avoiding wing-tip effects. Since the wind tunnel has a square cross-section (91.4 × 91.4 cm) this is easily achieved. A vertical mount allows liquid titanium tetrachloride ($TiCl_4$) to run down the entire span of the airfoil by means of gravity action. This liquid, which generates the smoke for flow visualization, is allowed to run down near either the leading or trailing edge prior to flow start-up. The smoke therefore visualizes an entire separating vortex sheet and its development during the course of the flow. To obtain an initial smoke sheet as homogeneous as possible it was necessary to clean the airfoil surface after each test run with soap and water and to carefully dry the clean surface. Otherwise a residue build-up interfered with homogeneous smoke generation and the quality of visualization became poor.

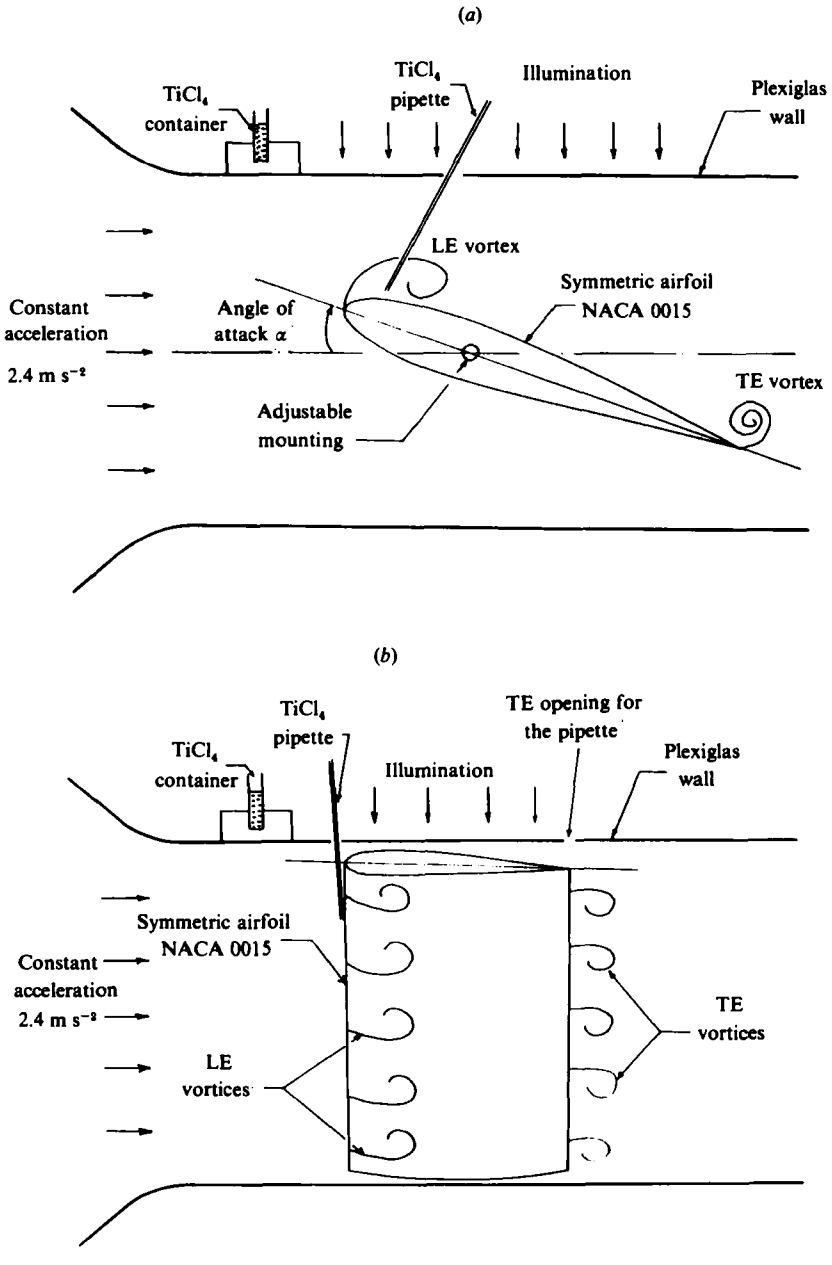

FIGURE 1. Sketch of experimental set-up; (*a*) set-up for chordwise visualization; (*b*) set-up for spanwise visualization.

No further modifications were needed. The angle of attack of the airfoil was adjustable from outside the tunnel. The flow acceleration was $a = 2.4$ m/s^2 after start from rest and was sustained for 4 seconds. This flow was achieved by proper control of the electric power feeding the fan motor as described by Freymuth *et al.* (1983*a*). Airfoils of different chord lengths c were available which allowed a variation in Reynolds number R, defined by

$$R = a^{\frac{1}{2}} c^{\frac{3}{2}} \nu^{-1}, \tag{1}$$

where ν is the kinematic viscosity of air. Flow after start-up was filmed over the mid-section of the airfoil span, looking at the suction side of the airfoil, with a Bolex camera at a rate of 64 frames per secod. Floodlighting was from the top of the tunnel.

3. Visualization of vortical patterns over the airfoil

It seems best to demonstrate the strengths and current limits of our flow-visualization method by means of examples selected on the basis of photographic resolution and their effectiveness in conveying a multitude of interesting patterns. This is not an exhaustive parametric study of pattern development.

3.1. *Chordwise versus spanwise visualization in the two-dimensional regime*

In figure 2 we display chordwise (top) and spanwise (bottom) visualizations of a vortical pattern as it occurs over the suction side of an airfoil at an instant in time after flow start-up and prior to the onset of turbulence. The airfoil for these complementary visualizations had a chord length $c = 15.2$ cm and faced the flow at an angle of attack $\alpha = 26°$. For both visualizations flow is from left to right as sketched in figure 1.

In the spanwise visualization of figure 2 (top) smoke outlines the contour of the suction side of the airfoil from approximately the leading edge at the left to the trailing edge situated to the right of a smoke bulge. Smoke leaves the trailing edge as a rather straight, slightly downward-sloping line. Above the airfoil surface an intricate vortex pattern can be seen which demonstrates the fine pattern resolution of this chordwise view. Since the airfoil surface has a shiny black anodized surface, a mirror image of the vortex pattern can also be seen facing downward, which should not be confused with an actual vortex pattern. The pressure side (bottom) of the airfoil was neither illuminated nor coated with smoke and therefore remains invisible in this view.

Figure 2 (bottom) visualizes the same vortex patterns as figure 2 (top) but in spanwise view. The airfoil span is in the vertical as sketched in figure 1(*b*) and a midspan section of the airfoil suction side is viewed. Smoke-generating liquid was allowed to run down along the leading edge of the airfoil. The leading edge can be seen as a faint vertical left boundary of illumination in the left part of the figure. The trailing edge is also visible as a vertical line of brightness approximately below the trailing edge as visualized in figure 2 (top). Additional vertical bands of brightness and darkness outline some of the vortical dimensions corresponding to vortex patterns of figure 2 (top) but fine details and ease of interpretation are lost in this projection. Therefore usefulness of this visualization is limited to providing evidence that the flow is two-dimensional at this stage. Spanwise visualization becomes more important during subsequent transition when the flow becomes three-dimensional. The next section will show this more clearly.

3.2. *Spanwise visualization of transition*

Transition over solid surfaces in steady flows has been visualized for thirty years. We were eager to obtain for the first time corresponding visualizations in a starting flow. In steady-flow visualization, conditions have been enhanced, usually by means of a vibrating ribbon. We refer to the pioneering papers by Fales (1955) and Hama, Long & Hegarty (1957), Hama (1959, 1960) and Hama & Nutant (1963) and to a recent paper by Saric & Thomas (1984). A flow pulse from a small hole has enhanced the visualizations by Gad-el-Hak, Blackwelder & Riley (1981) and Perry, Lim & Teh

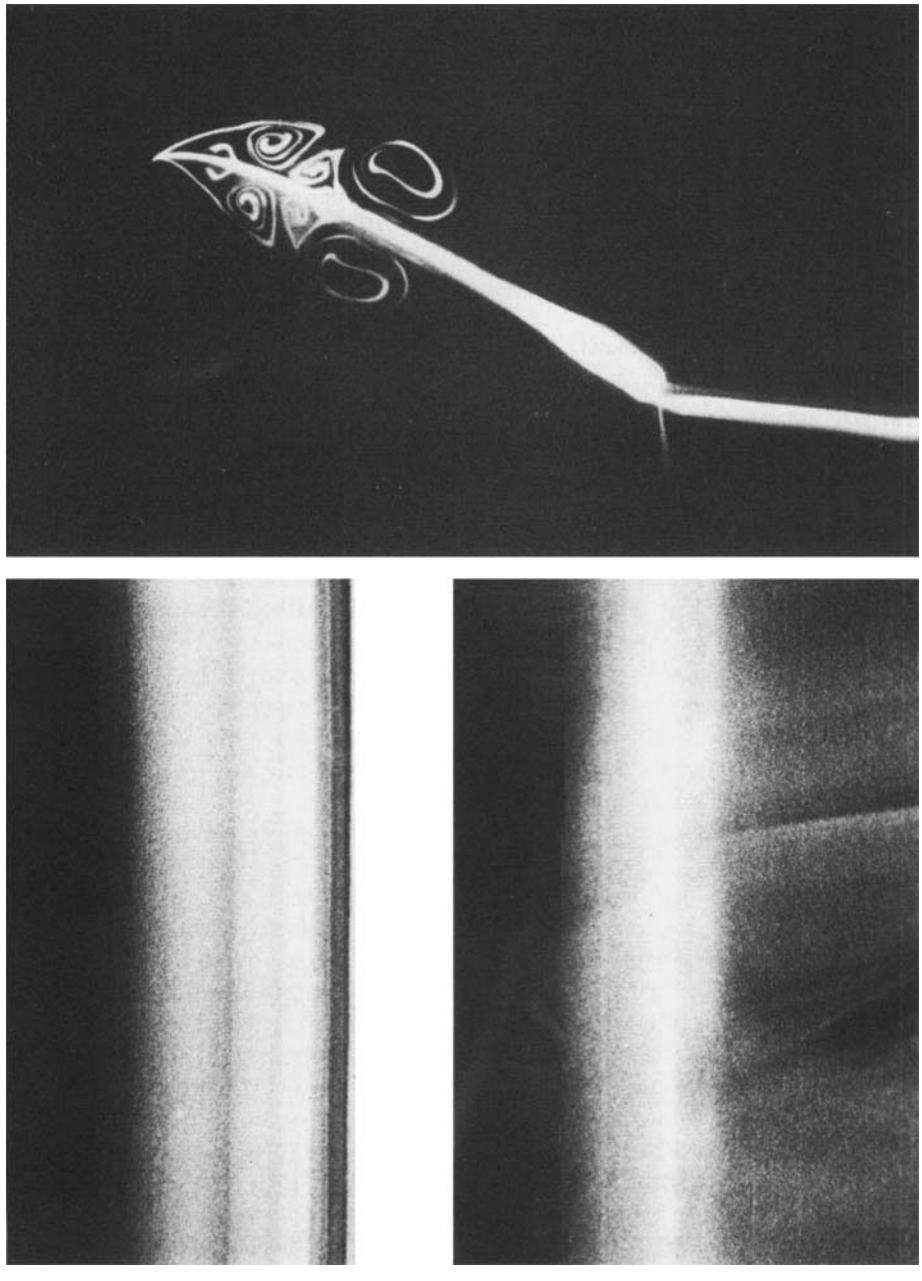

FIGURE 2. Chordwise view (top) versus spanwise view (bottom) of a vortical pattern over the airfoil, in the laminar regime; $\alpha = 26°$, $c = 15.2$ cm, $R = 5200$.

(1981). In accelerating flow such enhancements appeared questionable and we relied on the unaltered flow to reveal itself. This approach (among others) has been previously used by Brown (1965) and by Mueller (1983) in flows over ogive bodies and by Gad-el-Hak *et al.* (1984) in a decelerating flow over a flat plate.

Figure 3 shows a movie sequence of spanwise visualizations at $\alpha = 10°$, $c = 71$ cm. Frames are ordered from top to bottom and from left to right. The time between

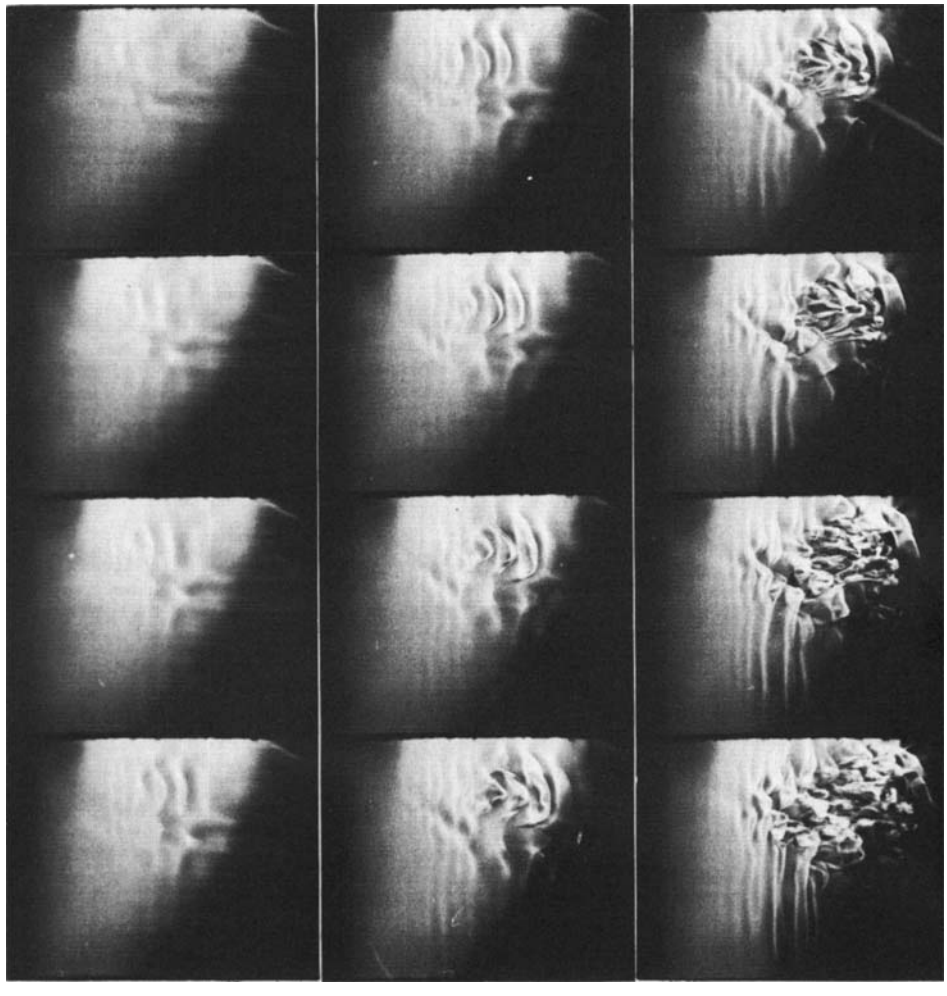

FIGURE 3. For caption see p. 244.

consecutive frames in this figure is $\Delta t = \frac{1}{64}$ s. The time from flow start-up to the first frame of a sequence $t_1 = \frac{72}{64}$ s for this sequence. The leading edge is visible in each frame as the left vertical boundary of illumination, close to the left frame edge. The airfoil extends beyond the right frame edge, i.e. the trailing edge has not been visualized. To get a feel for the geometrical scale of visualization the physical frame height is labelled h and in this figure is 48 cm. This compares with a tunnel height of 91.4 cm. Let us now describe the vortical developments visualized in this sequence. From a background of weak, nearly two-dimensional waves, a turbulent spot emerges in figure 3(*a*), starting from a few horseshoe vortices. These vortices go through the characteristic Λ and Ω shapes previously recognized by Hama & Nutant (1963) in a steady flow. The spot quickly grows by adding more horseshoe vortices while the two-dimensional background becomes stronger. The spot grows quickly beyond the frame size. The V-shape of the left boundary of the spot becomes a more two-dimensional shape in figure 3(*b*). Near the leading edge, two-dimensional vortices are released incessantly. As they move into the spot, these two-dimensional vortices

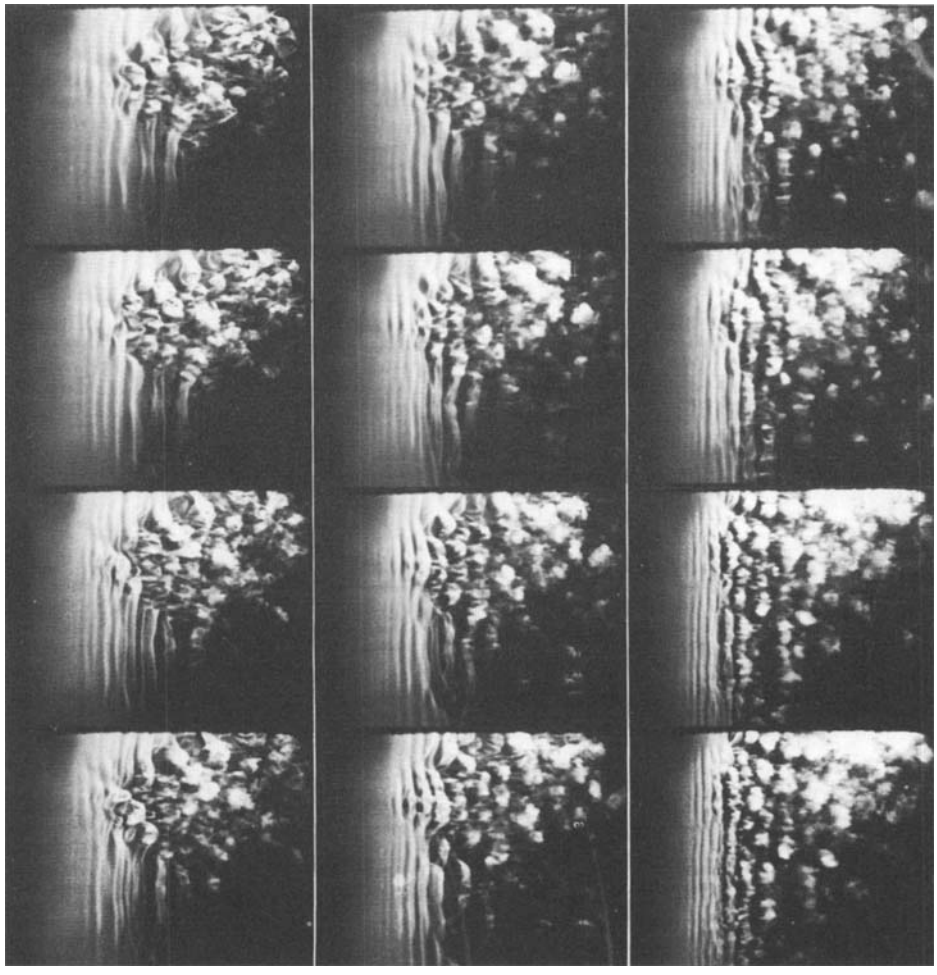

FIGURE 3. Initial development of a turbulent spot over the airfoil at $\alpha = 10°$, $c = 71$ cm, $R = 52400$, $\Delta t = \frac{1}{64}$ s, $t_1 = \frac{72}{64}$ s, $h = 48$ cm.

become extremely corrugated, presumably by innumerable horseshoe vortices which slip over or wrap around them. This condition carries the vortices into the turbulent regime, which is characterized by the diffuseness of the smoke. The sequence of figure 3 is our best for showing development of a turbulent spot. The sequence has nevertheless some flaws: illumination in the lower right corner of each frame was inadequate; and better space–time resolution would be desirable. However, such resolution of the initiation of a turbulent spot has not been attained previously, even in steady flow and with artificial local stimulation.

Figure 4 shows three-dimensional developments for the same airfoil but at a higher angle of attack $\alpha = 20°$. At this higher angle the initial two-dimensional vortices become stronger before they break down into arrays of aligned or staggered horseshoe vortices, similar to the ones observed by Hama & Nutant (1963), Perry *et al.* (1981) and Saric & Thomas (1984) in a steady flow with vibrating-ribbon stimulation. The development of corrugation of two-dimensional vortices near the leading edge shows up more clearly than in figure 3 and is presumably due to horseshoe vortices wrapping around it.

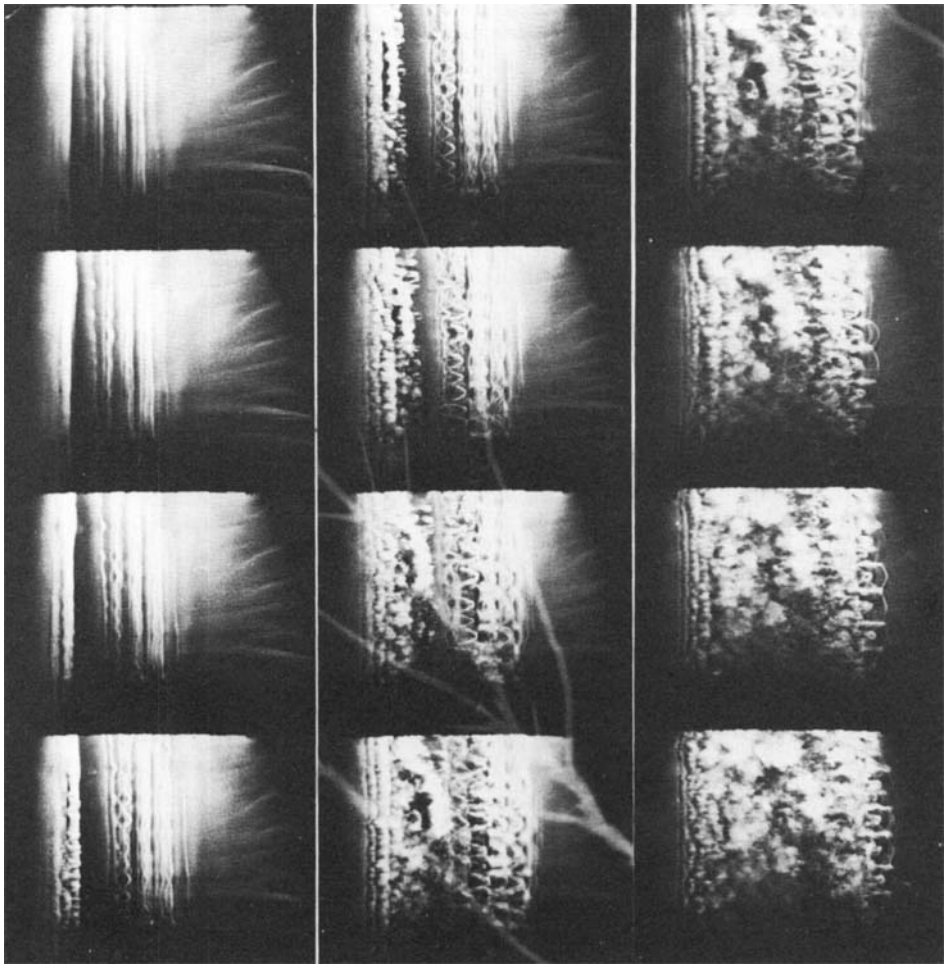

FIGURE 4. Transition over the airfoil at $\alpha = 20°$, $c = 71$ cm, $R = 52400$, $\Delta t = \frac{1}{64}$ s, $t_1 = \frac{64}{64}$ s, $h = 48$ cm. The electrostatic discharge in the middle column happened in the film-developing laboratory and was beyond our control.

Figure 5 (top) displays diamond-shaped linking of vortices at $\alpha = 20°$, $c = 15.2$ cm similar to patterns found by Saric & Thomas (1984) in steady flow over a flat plate under forced conditions. Actually, vortex linking was first identified by Clark & Kit (1980) in a free shear layer from a sharp-edged orifice. Linking can be interpreted as a piecewise pairing process, in contrast to the more regular initial pairing visualized by Freymuth (1966). In periodic situations, linking-like pairing gives rise to subharmonics although more weakly, since it is a weaker, partial form of pairing.

Figure 5 (middle), taken from another sequence at $\alpha = 80°$, captures pairing of a vortex filament with its two adjacent neighbours and rapid crossover from one neighbour to the other, in the left half of the frame. Ten frames later in the same sequence vortical interactions are more global and patterns resemble a loosely woven fabric as shown in figure 5 (bottom).

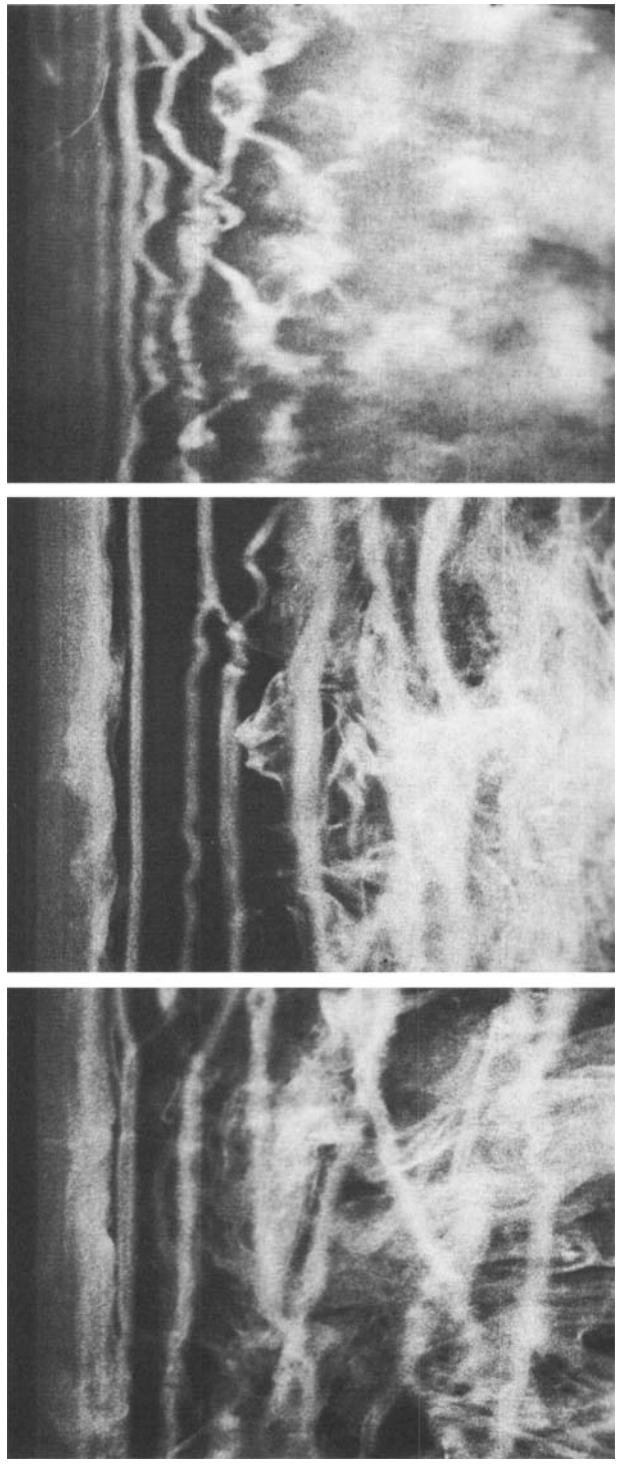

FIGURE 5. Top: diamond patterns at $\alpha = 20°$, $c = 15.2$ cm, $R = 5200$, $t_1 = \frac{97}{64}$ s. Middle: crossover of a vortex filament between neighbours at $\alpha = 80°$, $c = 15.2$ cm, $R = 5200$, $t_1 = \frac{66}{64}$ s. Bottom: more-global vortical interactions at $\alpha = 80°$, $c = 15.2$ cm, $R = 5200$, $t_1 = \frac{76}{64}$ s. In each case $h = 19$ cm.

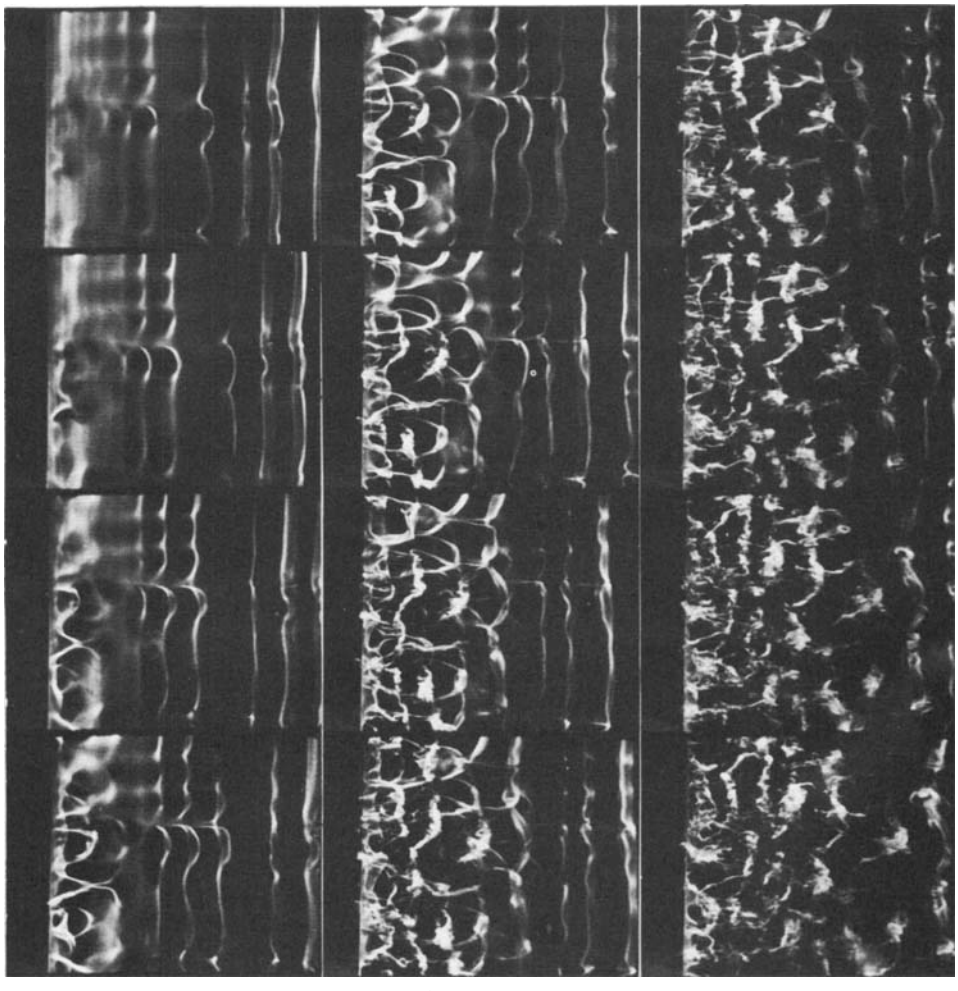

FIGURE 6. Vortex linking behind the trailing edge of the airfoil at $\alpha = 20°$, $c = 35.6$ cm, $R = 18250$, $\Delta t = \frac{1}{64}$ s, $t_1 = \frac{54}{64}$ s, $h = 32$ cm.

4. Visualization of vortical patterns behind the trailing edge

Vortices separating from the trailing edge have an opposite sense of rotation to the leading-edge vortices and encounter less wall influence. The single sequence of three-dimensional pattern development presented in figure 6 may suffice to show this. Vorticity moves to the right and is shed from the trailing edge, visible as the left boundary of illumination. A process of vortex linking resembling a chain-link fence is dramatically apparent, prior to more turbulent developments. The sequence was taken behind the trailing edge at $\alpha = 20°$, $c = 35.6$ cm and the frame height was $h = 32$ cm.

5. Conclusions

A simple modification to our visualization methods allowed for the first time the visualization of three-dimensional vortex patterns in a starting flow. We have

identified some new processes and on occasion surpassed pattern resolution obtained in other flow configurations.

The technical assistance of Mr R. Meinzer is acknowledged. This work has been supported by AFOSR grant number 81-0027; Dr J. McMichael was the programme manager.

REFERENCES

BROWN, F. N. M. 1965 The physical model of boundary layer transition. In *Proc. 9th Midwestern Mechanics Conf., U. of Wisconsin*, p. 421.

CLARK, J. A. & KIT, L. 1980 Shear layer transition and the sharp-edged orifice. *Trans. ASME* I: *J. Fluids Engng* **102**, 219.

FALES, E. N. 1955 A new laboratory technique for the investigation of the origin of fluid turbulence. *J. Franklin Inst.* **259**, 491.

FREYMUTH, P. 1966 On transition in a separated laminar boundary layer. *J. Fluid Mech.* **25**, 683.

FREYMUTH, P., BANK, W. & PALMER, M. 1983*a* Visualization of accelerating flow around an airfoil at high angles of attack. *Z. Flugwiss. Weltraumforschung* **7**, 392.

FREYMUTH, P., BANK, W. & PALMER, M. 1983*b* Use of titanium tetrachloride for visualization of accelerating flow around airfoils. In *3rd Intl Symp. on Flow Visualization, Ann Arbor, Sept. 6–9, Preprint volume*, p. 800.

FREYMUTH, P., BANK, W. & PALMER, M. 1984 Vortices around airfoils. *Am. Scient.* **72**, 242.

FREYMUTH, P., BANK, W. & PALMER, M. 1985 Further experimental evidence of vortex splitting. *J. Fluid Mech.* **152**, 289.

GAD-EL-HAK, M., BLACKWELDER, R. F. & RILEY, J. J. 1981 On the growth of turbulent regions in laminar boundary layers. *J. Fluid Mech.* **110**, 73.

GAD-EL-HAK, M., DAVIS, S. H., MCMURRAY, J. T. & ORSAG, S. A. 1984 On the stability of the decelerating laminar boundary layer. *J. Fluid Mech.* **138**, 297.

HAMA, F. R. 1959 Some transition patterns in axisymmetric boundary layers. *Phys. Fluids* **2**, 664.

HAMA, F. R. 1960 Boundary-layer transition induced by a vibrating ribbon on a flat plate. In *Proc. 1960 Heat Transfer and Fluid Mechanics Institute*, p. 92. Stanford University Press.

HAMA, F. R., LONG, J. D. & HEGARTY, J. C. 1957 On transition from laminar to turbulent flow. *J. Appl. Phys.* **28**, 388.

HAMA, F. R. & NUTANT, J. 1963 Detailed flow-field observations in the transition process in a thick boundary layer. In *Proc. 1963 Heat Transfer and Fluid Mechanics Institute*, p. 77. Stanford University Press.

MUELLER, T. J. 1983 Flow visualization by direct injection. In *Fluid Mechanics Measurements* (ed. R. J. Goldstein), p. 307. Hemisphere.

PERRY, A. E., LIM, T. T. & TEH, E. W. 1981 A visual study of turbulent spots. *J. Fluid Mech.* **104**, 387.

SARIC, W. S. & THOMAS, A. S. W. 1984 Experiments on the subharmonic route to turbulence. In *Turbulence and Chaotic Phenomena in Fluids*. IUTAM (ed. T. Tatsumi), p. 117. Elsevier.